Computer aided location of avalanche victims with ground penetrating radar mounted on a helicopter.

M. Haltmeier[1,2], R. Kowar[1], and O. Scherzer[1].

[1] Department of Computer Science, University of Innsbruck.

[2] alpS - Center for Natural Hazard Management, Innsbruck.

Corresponding e-mail address: `Markus.Haltmeier@uibk.ac.at`.

Abstract:
Ground penetrating radar (GPR) utilizes the reflection of electromagnetic waves for high resolution imaging of shallow subsurface structures. The goal of this paper is to study the potential of using GPR in combination with pattern recognition for rapid location of avalanche victims. Real world experiments and simulations have shown that avalanche victims reflect radar waves and appear as diffraction hyperbolas in the recorded radar data. This paper deals with a two level algorithm based on a fast active contour method and a matched filter for computer aided locating of diffraction hyperbolas.

1 Introduction and motivation

GPR relies on the reflection of electromagnetic waves on discontinuities [4]. In contrast to radar detection of aircrafts in the sky the radar antennas are moved over the surface rather than rotated around a center. The various applications of GPR include archeological research and landmine and pipeline detection [6].

In the GPR technology a short electromagnetic pulse is emitted from a transmitting antenna. The induced electromagnetic wave propagates unhindered until it collides with structures of different electromagnetic properties. The scattered electromagnetic field is then detected with a receiving antenna and represented in radargrams.

We apply the GPR technology for locating avalanche victims mounted on a flying helicopter under the reasonable assumption that the background media consists of the three different regions air, snow and subsurface. Consequently in the radargram there appear reflections caused by jumps in the value of the background velocity of propagation and reflections on small buried objects [10]. A small buried object manifests itself as a diffraction hyperbola. The idea of using GPR for location of avalanche victims is not new [9]. However there was a need for experts who sought for diffraction hyperbolas in the radargrams. In contrast to former research this paper is concerned with the development of a real-time software package for *semi-automatic locating of avalanche victims* with radar technology from helicopters.

Our algorithm consists of two steps. First we adopt a parametric active contour method [2, 12]

for automatic extraction of the snow layer. Such an active contour approach has not been used in the processing of GPR data so far. For enhancing diffraction hyperbolas in radargrams we use a *matched* filter algorithm. We note that the optimal choice of a template diffraction hyperbola that is compared with the radar data is crucial. In Section 2 we present results of our simulations of diffraction patterns of extended objects.

This paper is organized as follows: In Section 2 we describe the collecting of radar data sets and introduce the two level algorithm for computer aided location of avalanche victims. The applied preprocessing is presented in Section 3. Details on the active contour algorithm used to extract the snow layer are given in Section 4 and in Section 5 we present the matched filter algorithm. Results of the algorithm applied to real life data show its potential and robustness. Finally in Section 6 we discuss limitations and possible further improvements.

2 The nature of radar reflection data and simulation of radargrams

In this Section we describe the collecting of radar data sets. For simplicity of the presentation we assume, that the helicopter with the emitting and receiving radar dipole-antenna travels on the straight line $\mathbf{x}_{\text{ant}} := (x_{\text{ant}}, 0, 0)$ and that the diploe-antennas point in direction of motion $\mathbf{e} := (1, 0, 0)$. The left image in Figure 1 illustrates the basic principle of transmission, reflection and recording of radar pulses out of a flying helicopter.

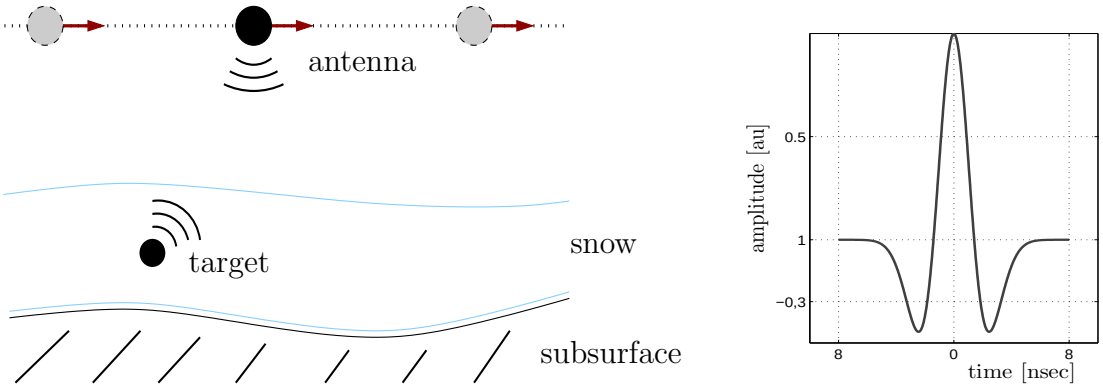

Figure 1: ***Principal of collecting radar data.*** **Left image: At each position the radar antenna emits a short radar pulse. The induced electromagnetic wave gets reflected, and the scattered signals are recorded and collected in radagrams. Right image: Temporal shape of the emitted electromagnetic pulse.**

At each position $\mathbf{x}_{\text{ant}}$ the radar dipole-antenna emits a short electromagnetic pulse. According to [11] the electric field component of the emitted radar wave at location $\mathbf{x}$ and time $\hat{\tau}$ is given by

$$\mathbf{E}_{\text{ant}}(\mathbf{x}, \hat{\tau}) = \mathbf{e}\, \frac{\sin(\theta) w_{\text{ant}}\left(\hat{\tau} - |\mathbf{x} - \mathbf{x}_{\text{ant}}|\,/c\right)}{|\mathbf{x} - \mathbf{x}_{\text{ant}}|}\,. \tag{1}$$

Here θ is the angle between $\mathbf{e}$ and $\mathbf{x} - \mathbf{x}_{\text{ant}}$, w_{ant} is the temporal shape of the emitted radar

pulse, and c denotes the velocity of propagation in air. The function w_{ant} represents the spectral characteristics of the used dipole antenna [11] and can be approximated by the second derivative of a small Gaussian, see Figure 1.

The electromagnetic pulse propagates trough the background media and is reflected at scatterers, that hold different electromagnetic properties (cf. Figure 1). The scattered electric field

$$\mathbf{E}_{\text{scat}}(\mathbf{x}, \hat{\tau}) = \mathbf{e}\big(E_1(\mathbf{x}, \hat{\tau}) + E_{\text{ob}}(\mathbf{x}, \hat{\tau}) + E_2(\mathbf{x}, \hat{\tau})\big) \tag{2}$$

at position $\mathbf{x}$ and time $\hat{\tau}$ is the sum of the field $\mathbf{e}E_1(\mathbf{x}, \hat{\tau})$ scattered on the interface between air and snow, reflections $\mathbf{e}E_{\text{ob}}(\mathbf{x}, \hat{\tau})$ resulting from objects within in the snow layer, and the field $\mathbf{e}E_2(\mathbf{x}, \hat{\tau})$ scattered on the interface between snow and subsurface. For simplicity we assume that the scattering of radar waves does not change the polarization vector $\mathbf{e}$.

The receiving antenna at location $\mathbf{x}_{\text{ant}}$ is modeled as projecting the scattered field $\mathbf{E}_{\text{scat}}(\mathbf{x}_{\text{ant}}, \cdot)$ onto the axis $\mathbf{e}$ followed by the convolution $*$ in time with w_{ant}. The one dimensional signal

$$u_0(x_{\text{ant}}, \cdot) := (\mathbf{E}_{\text{scat}}(\mathbf{x}_{\text{ant}}, \cdot) \cdot \mathbf{e}) * w_{\text{ant}} \tag{3}$$

is recorded within the time window $\hat{\tau} \in [0, \hat{\tau}_{\text{end}}]$ and is called **a-scan**.

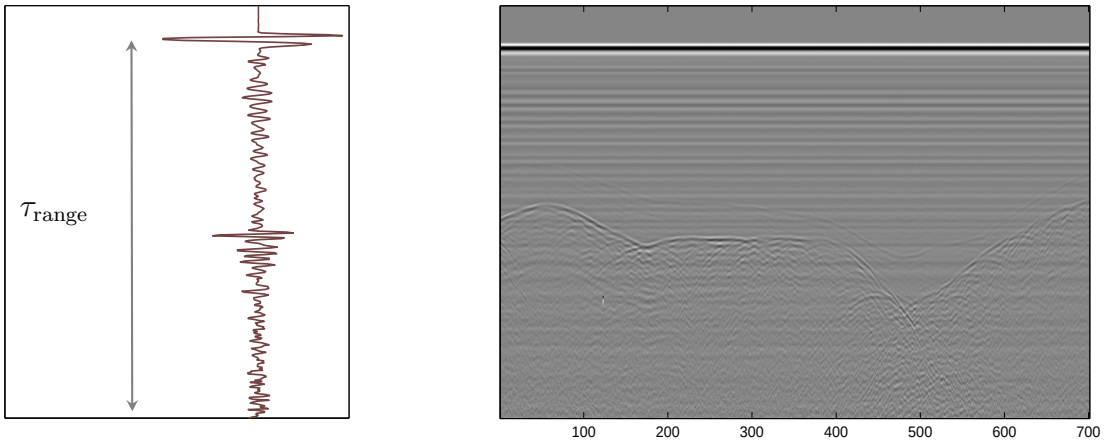

Figure 2: ***Example of radar raw data collected in St. Anton am Arlberg.*** **The left image shows a-scan signal recorded within the time window** $[0, \tau_{\text{range}}]$**. The right image shows a radargram.**

By varying $x_{\text{ant}} \in [0, x_{\text{end}}]$ and after using the re-scaling $x = x_{\text{ant}}/x_{\text{end}}$, $\tau = \hat{\tau}/\hat{\tau}_{\text{range}}$ the radar data set forms a two dimensional gray-scale image

$$u_0 : [0,1] \times [0,1] \to \mathbb{R} : \quad (x, \tau) \mapsto u(x, \tau)\,,$$

which is called **radargram**. A small buried object manifests itself in the radargram as a **diffraction hyperbola**. Figure 2 shows an example of an a-scan and a radargram gathered

during a field experiment in St. Anton am Arlberg in Tyrol, Austria in early 2005 [7]. Here the central wavelength of the used dipole antenna is approximately 0.3 meters. The radargram contains a small diffraction hyperbola descending from the reflections of a buried object that almost disappears between clutter and noise.

To substantiate the relation between targets and the corresponding diffraction hyperbolas we performed extensive simulations of radargrams based on Huygens principle [13]. We note that only a point scatterer in the idealized situation of homogenous non-absorbing background gives an exact hyperbola. Two examples of diffraction patterns of extended objects are illustrated in Figure 3. Furthermore the refraction of radar waves on a curved air-snow interface causes displacement between the horizontal position of a target and its diffraction hyperbola. We conclude that a diffraction hyperbola in the snow layer is a definite indicator for the presence of a buried object and can be used to narrow large avalanche cones down to certain small areas of suspicious.

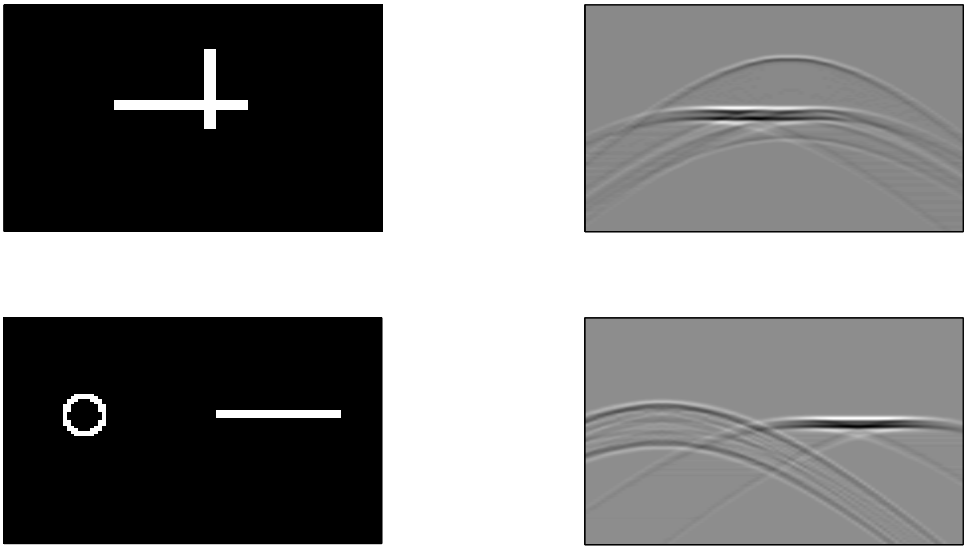

Figure 3: ***Simulated diffraction patterns of non-punctual objects assuming horizontal air-snow interface.*** **The first column shows two velocity profiles (depth versus x) and the second column shows the corresponding radargrams (τ versus x). The extend of the imaged objects is several times larger than the central wavelength of the used dipole-antenna.**

We note that in this paper we do not touch the problem of discriminating between human victims and debris, such as trees or rocks [10]. Our aim is to produce a pseudo-image of the snow layer that peaks at the vertex of a diffraction hyperbola. We proceed as follows: After removing clutter and noise we extract the reflections coming from within the snow. Finally a matched filter algorithm is applied to detect diffraction hyperbolas.

3 Preprocessing and the removal of clutter and noise

In this Section we give some details on the applied preprocessing [4]. In practical applications the radargram is sampled at $\mathtt{x}[\mathtt{i}] := (\mathtt{i}-1)/(\mathtt{N}-1)$ and $\mathtt{tau}[\mathtt{j}] := (\mathtt{j}-1)/(\mathtt{N}-1)$ for $\mathtt{i},\mathtt{j} \in \{1,\ldots,\mathtt{N}\}$, and we denote the digitalizes radargram by

$$\mathtt{u_0}[\mathtt{i},\mathtt{j}] := u_0(\mathtt{x}[\mathtt{i}],\mathtt{tau}[\mathtt{j}])\ , \quad \mathtt{i},\mathtt{j} = 1,\ldots,\mathtt{N}\ .$$

For simplicity we assume that the number of a-scans is equal to the number $\mathtt{N}$ of time samples. Here all models are presented in a continuous setting and implemented after discretization.

The actual radargram (see Figure 2) decomposes into the sum

$$u(x,\tau) = u_0(x,\tau) + u_c(x,\tau) + u_n(x,\tau)$$

of the wanted signal $u_0(x,\tau)$, the clutter $u_c(x,\tau)$ and the noise $u_n(x,\tau)$. In the GPR community the term **clutter** is used to characterize signal components that contain the spectral characteristics of the dipole antenna but are not correlated with scattering from buried objects [4]. Clutter occurs from multiple reflections on fixed structures and reflections resulting from the inhomogeneous background. Separating out the clutter from the target signals is a main factor in the successful interpretation of the GPR data and is an active research area [5, 17, 3].

In our application the main part of disturbing signals consists of horizontal lines, presumably resulting from multiple reflections on the helicopter (cf. Figure 2). In this case **mean a-scan subtraction** [4, p.27]

$$\bar{u}(x,\tau) := u(x,\tau) - \int_0^1 u(x,\tau)\,dx \tag{4}$$

is a good technique to reduce clutter. Another advantage of this classical clutter reduction method is that equation (4) can be implemented with $\mathcal{O}(\mathtt{N}^2)$ operations. This fact is important since we have a real-time application in mind. The left image in Figure 4 shows the filtered radargram $\bar{u}(x,\tau)$ after removing clutter and noise.

4 Automatic extraction of the snow layer by combining tube methods with parametric active contours.

In this Section we present an active contour model that we apply to automatically locate the boundaries of the snow layer. Parametric active contour models are extensively used to locate object boundaries in images [2, 12]. Many real life application of computer vision including segmentation [1], motion tracking [15] and shape modeling [18] are based on active contour models.

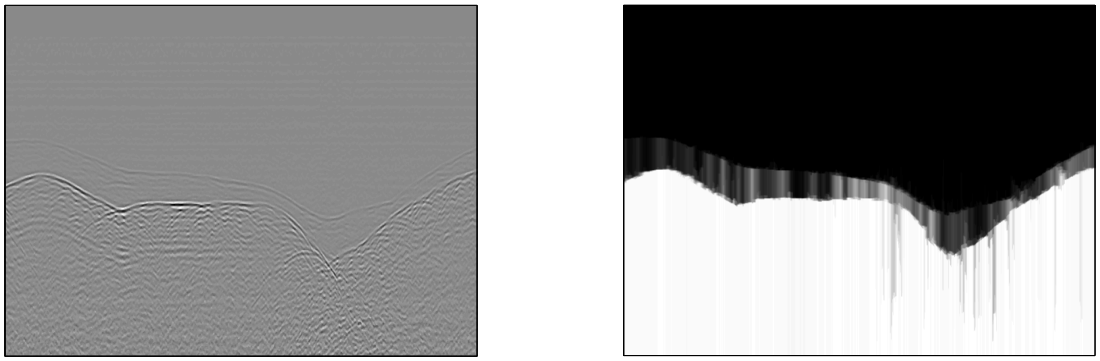

Figure 4: Left: Radargram after removing clutter and noise. Right: Result of minimizing the BV functional (5) for each column of the radargram.

The radargram $\bar{u}(x,\tau)$ mainly decomposes into three separate regions that are characterized by the absolute value of the *average amplitude*. The average amplitude depends on a scale parameter λ and is defined by

$$\Phi_\lambda(x,\cdot) := f_\lambda\,,$$

where $f_\lambda : [0,1] \to \mathbb{R}$ is the minimizer of the one dimensional BV functional

$$\int_0^1 \Big(f(\tau) - |\bar{u}(x,\tau)|\Big)^2\, d\tau + \lambda \int_0^1 |f'(\tau)|\, d\tau\,. \tag{5}$$

Here the prime $'$ denotes the derivative with respect to time. Note that (5) can be minimized immediately after taking a single a-scan and therefore allows a dynamic implementation during the helicopter flight. For the numerical implementation we used $\lambda = 5/2 \cdot \|\bar{u}(x,\cdot)\|_{L^2(\mathbb{R})}$. The large magnitude of the scale parameter λ assures that the minimizer f_λ of (5) is a monotone increasing function that only jumps at the boundaries of the snow layer.

The functional (5) can be minimized with tube methods [16, 8] with $\mathcal{O}(\mathtt{N})$ operations. This leads to an $\mathcal{O}(\mathtt{N}^2)$ algorithm for the calculation of the amplitude image Φ_λ. The right image in Figure 4 shows the result of the tube method applied column by column to the radargram on its left.

The boundaries of the snow layer correspond to the edges within the image Φ_λ to which we apply the parametric active contour. A parametric active contour is an evolving family $\big(c_\nu\big)_{\nu>0}$ of planar curves $c_\nu : [0,1] \to [0,1]^2$ such that c_ν tends to a local minimizer of the **energy functional**

$$\mathcal{E}_{\mathrm{pot}}(c) + \frac{\alpha}{2}\int_0^1 \left(\frac{\partial c}{\partial s}\right)^2 ds + \frac{\beta}{2}\int_0^1 \left(\frac{\partial^2 c}{\partial^2 s}\right)^2 ds\,, \tag{6}$$

for $\nu \to \infty$ [19]. Here the parameters α and β control the smoothness of the active contour whereas the potential $\mathcal{E}_{\mathrm{pot}}(c)$ depends on the amplitude Φ_λ and attracts the active contour to the wanted boundaries.

In our application the boundaries can be expressed as graphs of functions $\tau = h(x)$. This motivates us to introduce the energy functional

$$\mathcal{E}(h) = \int_0^1 \Big(-\gamma h(x) + \Phi_\lambda(x, h(x))\Big)\, dx + \frac{\alpha}{2} \int_0^1 h'(x)^2\, dx \tag{7}$$

defined for real valued functions h instead of using the functional (6) defined for curves c. Here γ is an additional parameter. The left picture in Figure 5 illustrates the construction of the potential $\tau \mapsto -\gamma \cdot \tau + \Phi_\lambda(x, \tau)$ for fixed x.

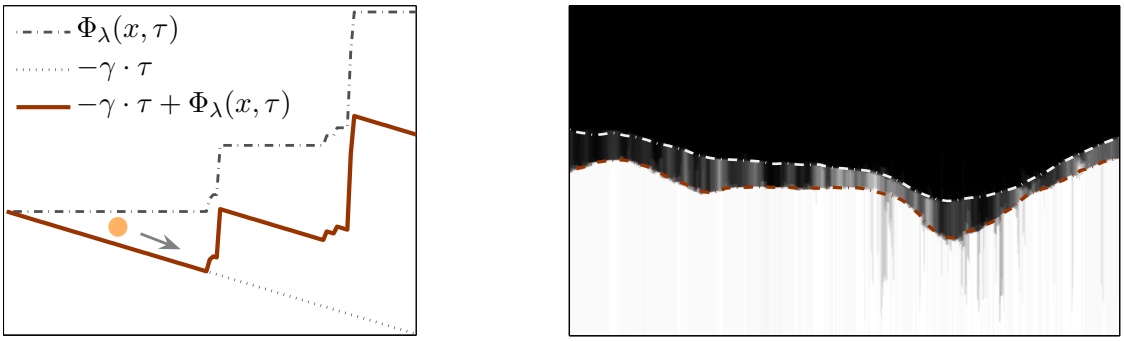

Figure 5: ***Active contour algorithm for detection of the snow boundaries.*** **The left image illustrates the term $-\gamma \cdot \tau + \Phi_\lambda(x, \tau)$ in (7) that attracts the active contour to the wanted boundaries. The right image shows the boundaries of the snow layer found by our algorithm.**

The optimality condition for locally minimizing (7) attains the form

$$\nabla \mathcal{E}(h) = -\gamma + (\partial \Phi_\lambda / \partial \tau)(x, h(x)) - \alpha h''(x) = 0\ ,$$

which is solved iteratively by the **steepest descent** method. Thus we define

$$h_{i+1}(x) = h_i(x) + ds \cdot \Big(\gamma - (\partial \Phi_\lambda / \partial \tau)(x, h(x)) + \alpha h_i''(x)\Big)\ , \quad i \in \mathbb{N} \tag{8}$$

with some initial guess h_0. In the numerical implementation iteration (8) is applied approximately $\mathtt{N}$ times and the derivative $\partial \Phi_\lambda / \partial \tau$ of Φ_λ with respect to the second variable is implemented with central differences. Hence the overall cost of the active contour algorithm is $\mathcal{O}(\mathtt{N}^2)$.

Figure 5 shows the boundaries $h_1(x)$, $h_2(x)$ of the snow layer that are found by our algorithm. Finally we define $u_S = \bar{u} \cdot \chi_S$, where χ_S is the characteristic function of

$$S := \{(x, \tau) : h_1(x) \le \tau \le h_2(x)\}\ .$$

5 Matched filter for the enhancing of diffraction hyperbolas.

In this Section we apply a matched filter algorithm to enhance the location of diffraction hyperbolas. A matched filter algorithm compares an original image with a template and

indicates where two features are most likely to correspond. In our application we apply the matched filter to the extracted radargram u_S, which only includes reflections coming from within the snow. The template is a radargram m of a single scatterer (diffraction hyperbola).

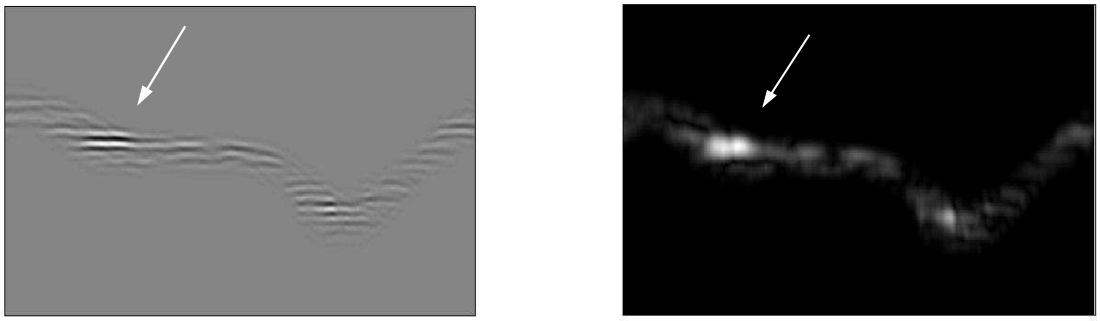

Figure 6: Results of the matched filter. The left image shows the result of the matched filter applied to the data seen in Figure 4 and the right image shows its envelope. The arrow points to a bright spot that corresponds to a diffraction hyperbola indicating an avalanche victim.

The heart of any concrete implementation of a matched algorithm is the definition of measure of similarity of two images. A typical measure is the squared **Euclidian distance**

$$\int_0^1 \int_0^1 \big(u_S(x,\tau) - m(x-x_0,\tau-\tau_0)\big)^2 \, dx\, d\tau \tag{9}$$

between the image u_s and the template m positioned at (x_0,τ_0). If U denotes the support of the template and $\int_U u(x+x_0,\tau+\tau_0)dxd\tau$ is approximately constant then the magnitude of the distance measure (9) is determined by the **convolution** term [14]

$$(u_S \star m)(x_0,\tau_0) := \int_0^1 \int_0^1 u_S(x,\tau) m(x-x_0,\tau-\tau_0)\, dx\, d\tau \; . \tag{10}$$

According to the Fourier convolution theorem (10) can be evaluated with the `FFT` algorithm in $O(\mathtt{N}^2 \log \mathtt{N})$ operations.

Figure 6 shows the result after applying the matched filter and its envelope, which is also calculated on the basis of the `FFT` algorithm. The bright spot correspond to a diffraction hyperbola indicating an avalanche victim. It's worth to compare the results of Figure 6 with the radargrams plotted in Figures 2 and 4, where the diffraction hyperbola is hardly visible. Figure 7 shows a further example where our algorithm is applied to a real life data set and where it again detects a diffraction hyperbola.

6 Discussion and outlook.

In this paper we presented a two level algorithm based on parametric active contours and matched filters to enhance diffraction hyperbolas in radargrams. We illustrated its potential for locating avalanche victims by applying it to real life data.

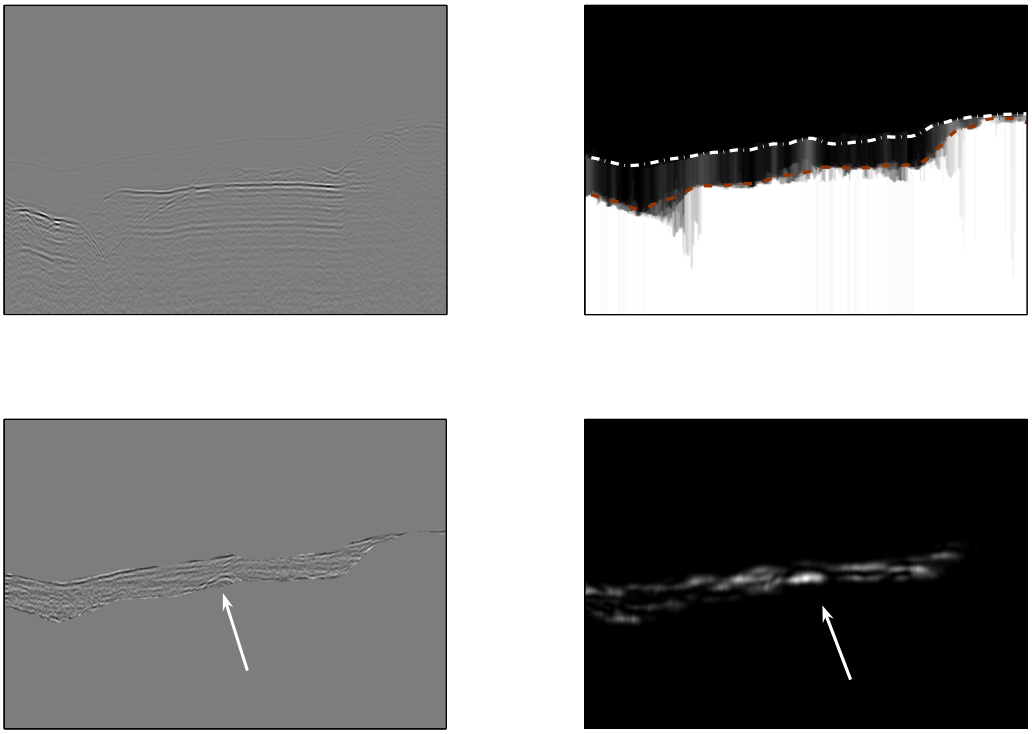

Figure 7: ***Further results of our algorithm applied to real life data.*** **Top left: Radargram after removing clutter and noise. Top right: Boundaries of the snow layer. Bottom left: Modified radargram that only contains reflections coming from within the snow. Bottom right: Envelope after applying the matched filter. The white arrows point to a hyperbola enhanced by our algorithm.**

For extracting the reflections coming from within the snow we proposed an active contour model that uses a real valued function instead of an arbitrary planar curve. The current version includes only the average amplitude Φ_λ to distinguish between different layers. If the reflections coming from within the snow are very weak our algorithm can fail. Therefore we intend to incorporate the texture of the radargram into the active contour algorithm. This should guaranty us to reliable find the boundaries of the snow layer.

For the actual imaging process we used a matched filter algorithm with a single template diffraction hyperbola. Based on our simulations and free-air experiments, we will decide if a single template hyperbola and more sophisticated (e.g. statistical) measures are able to discriminate between human victims and debris such as trees or rocks.

Acknowledgement

This work has been supported by alpS - Center for Natural Hazard Management in Tyrol in corporation and Wintertechnik Engineering Ltd. We want to thank Bardenz Bock Geo-

radar company (Germany) for making their GPR equipment and expert knowledge available. Moreover we thank Achim Heilig from alpS - Center for Natural Hazard Management for performing measurements and providing real life data sets to us.

References

[1] G. Aubert, M. Barlaud, O. Faugeras, and S. Jehan-Besson. Image segmentation using active contours: calculus of variations or shape gradients? *SIAM J. Appl. Math.*, 63(6):2128–2154 (electronic), 2003.

[2] A. Blake and M. Isard. *Active Contours: The Application of Techniques from Graphics, Vision, Control Theory and Statistics to Visual Tracking of Shapes in Motion.* Springer-Verlag, Secaucus, USA, 1998.

[3] L. Borcea, G. Papanicolaou, and C. Tsogka. Interferometric array imaging in clutter. *Inverse Problems*, 21:1419–1460, 2005.

[4] D. Daniels. *Ground Penetrating Radar.* The Institution of Electrical Engineers, London UK, 2004.

[5] T. Dogaru and L. Carin. Time-domain sensing of targets buried under a rough air-ground interface. *IEEE Trans. Antennas and Prop.*, 46:360–372, 1998.

[6] X. Feng and M. Sato. Pre-stack migration applied to gpr for landmine detection. *Inverse Problems*, 2:99–115, 2004.

[7] M. Haltmeier and R. Kowar. Rapid location of avalanche victims with ground penetrating radar. *ECMI-Newsletter*, 39, 2006.

[8] W. Hinterberger, M. Hintermüller, K. Kunisch, M. von Oehsen, and O. Scherzer. Tube methods for BV regularization. *J. Math. Imaging Vision*, 19(3):219–235, 2003.

[9] A. Instanes, I. Lønne, and K. Sandaker. Location of avalanche victims with ground-penetrating radar. *Cold Regions Science and Technology*, 38(1):55–61, 2004.

[10] C. Jaedicke. Snow mass quantification and avalanche victim search by ground penetrating radar. *Surveys in Geophysics*, 24:431–445, 2003.

[11] K. Kark. *Antennen und Strahlungsfelder.* Friedr. Vieweg & Sohn Verlag, Wiesbaden, 2004.

[12] M. Kass, A. Witkin, and D. Terzopoulos. Snakes: Active contour models. *Int. J. of Computer Vision*, 1(4):321–331, 1987.

[13] R. Kowar, M. Haltmeier, and T. Riser. Rapid location of avalanche victims via ground penetrating radar from a helicopter part 1: Simulation of diffraction patterns in radgrams. *Preprint series of department of computer science and mathematics, University of Innsbruck No. 40*, pages 1–9, 2006.

[14] J.P. Lewis. Fast template matching. In *Vision interface*, pages 120–123, 1995.

[15] F. Leymarie and M.D. Levine. Tracking deformable objects in the plane using an active contour model. *IEEE Trans. Pattern Anal. Mach. Intell.*, 15(6):617–634, 1993.

[16] E. Mammen and S. van de Geer. Locally adaptive regression splines. *Ann. Statist.*, 25(1):387–413, 1997.

[17] A. Merwe and I. Gupta. A novel signal processing technique for clutter reduction in gpr measurements of small, shallow land mines. *IEEE Trans. Geosc. Rem. Sens.*, 28(2):2627–2637, 2002.

[18] D. Terzopoulos and K. Fleischer. Deformable models. *The Visual Computer*, 4:306–331, 1988.

[19] C. Xu and J.L. Prince. Snakes, shapes and gradient vektor flow. *IEEE Trans. Image Processing*, 7:359–269, 1997.